Composite Structures 245 (2020) 112327

Contents lists available at ScienceDirect

Composite Structures

journal homepage: www.elsevier.com/locate/compstruct

A comparative study on glass and carbon fibre reinforced laminated composites in scaled quasi-static indentation tests

Mohamad Fotouhi[a,*], Mahdi Damghani[b], Mun Choong Leong[c], Sakineh Fotouhi[d], Meisam Jalalvand[e], Michael R. Wisnom[c]

[a] University of Glasgow, School of Engineering, Glasgow G12 8QQ, UK
[b] Department of Engineering Design and Mathematics, University of the West of England (UWE), Bristol BS16 1QY, UK
[c] Bristol Composites Institute (ACCIS), University of Bristol, Bristol BS8 1TR, UK
[d] Department of Mechanical Engineering, University of Tabriz, Tabriz, Iran
[e] Department of Mechanical and Aerospace Engineering, University of Strathclyde, 75 Montrose Street, Glasgow G1 1XJ, UK

ARTICLE INFO

Keywords:
Carbon/epoxy
Glass/epoxy
Indentation
Impact
Delamination

ABSTRACT

This paper investigates the effect of fibre properties of composite structures on the mechanical performance and formation of low-velocity impact damage. Quasi-static indentation tests were conducted on a comprehensive set of scaled Quasi Isotropic (QI) S-glass/8552 epoxy and QI IM7-carbon/8552 epoxy laminates, comparing changes in both in-plane dimensions and fully three-dimensionally scaled cases. Due to the higher thickness of the S-glass laminates, the mechanical results were normalized by a thickness scaling rule to have a fair comparison between the mechanical behaviour. The results demonstrated that the shape of the load-displacement of the S-glass/epoxy laminates is similar to that of the IM7-carbon laminates, with evident changes in rigidity appearing due to the onset and propagation of delamination and final failure caused by fibre breakage. The S-glass/8552 epoxy laminates had smaller load drops, higher deflection and higher mechanical energy absorption before failure compared to the IM7-carbon/8552 epoxy laminates. X-ray computed tomography scanning revealed that delamination is the dominant failure mode for the investigated laminates, and the shape of delamination was influenced by the ply angles at the interfaces. Comparing the glass and carbon laminates, ultrasonic C-scan results indicated similar delamination damage size for the initiation stage, however the damage size was found to be dependent on the fibre properties and layup sequence in the propagation stage.

1. Introduction

The past three decades have seen a notable increase in the use of composite materials in various engineering fields such as aerospace, military and automotive industries. Applications of composites in these areas are typically to make light and strong structures. However, various damage mechanisms such as delamination, matrix cracking and fibre breakage have limited the operational life and load-bearing capacities of these materials. One of the most critical loading conditions for composite structures is impact. Specifically, low velocity impact (LVI) leads to Barely Visible Impact Damage (BVID) which significantly affects compressive strength. Hence, it is of great importance to understand and characterize damage evolution in these materials.

Many researchers have investigated LVI behaviour of composite materials [1–7]. LVI is defined as an impact event in which the contact time of an impactor is very long compared to the stress-wave propagation time (i.e., approximately static loading) [7]. However, a LVI test generally has only a short duration, making it hard to tell anything about the damage sequence. Compared to LVI, quasi-static indentation (QSI) is much easier: low acquisition rates suffice and there is an absence of oscillations. It is widely accepted that both quasi-static indentation and LVI tests give similar damage propagation within plies in many cases [8,9]. Therefore, for simplification, QSI is often used instead to allow to interrupt at different indentation values for damage inspection [10].

Several studies have been carried out to investigate the effects of various parameters on LVI behaviour of laminated composites [11–14]. Summarizing these studies, five different parameters have been investigated: in-plane dimensions, laminate thickness, lay-up configuration, fibre direction and material properties (fibre and matrix type) [11–15]. The dimensions of the laminate were considered the main parameter governing the behaviour of laminates under impact [11].

* Corresponding author.
E-mail address: mohammad.fotouhi@glasgow.ac.uk (M. Fotouhi).

https://doi.org/10.1016/j.compstruct.2020.112327
Received 30 March 2020; Accepted 3 April 2020
Available online 06 April 2020

Yang et al. [12] investigated the influence of geometrical parameters on the damage initiation threshold. The experimental tests revealed that the impact force required for damage initiation in specimens of the same in-plane dimensions, varies with $h^{1.5}$, where h is the laminate thickness. Moreover, the results showed that the damage threshold increased steadily with increasing projectile diameter, with the most essential changes being evident in the thinner laminates. Other studies on the effects of geometrical parameters on beam-like specimens [11,16] showed that increasing the length or thickness led to a change in failure mode and location of failure. Damage initiated with a top surface contact failure in the short thick beams, while a lower surface flexural failure was observed in the long thin beams. The subsequent damage development was found to depend strongly upon the energy-absorbing capability of the structure. Drop-weight impact tests were conducted on a range of circular panels as a more representative geometry. It was concluded that simple beam-like configurations do not necessarily predict the mode of failure in more complex structures.

Another important parameter affecting the initiation and propagation of delamination is lay-up configuration. Fuoss et al. [13] provided extensive data on the effects of layup on specimens that were not quasi-isotropic (QI), and the impact damage resistance of each configuration. It was recommended that angled plies (45° plies) should be placed near the surface and the difference in angle between each ply should be kept between 30° and 45°. A study by Yang and Cantwell [12] also supported this result with a decrease in the damage threshold and an increase in delamination area when the angles between plies were increased beyond 45°.

Abbiset et al. [14] carried out a comprehensive study on the effects of in-plane dimension and thickness on the load–displacement behaviour and damage evolution of uni-directional carbon fibre composites with QI layup. However, they did not study the effect of material properties, especially the fibre modulus and failure strain, which are important factors for the damage evolution and load–displacement behaviour of laminates under LVI. Higher strength fibres provide higher load carrying capacity whilst higher failure strain provides a larger deformation before final failure potentially leading to enhanced energy absorption.

Carbon Fibre Reinforced Polymers (CFRP) and Glass Fibre Reinforced Polymers (GFRP) composites are being used as load bearing structural components in various industries. Despite considerable work in the literature regarding LVI behaviour and quasi-static indentation test on GFRP [16], CFRP [17,18], and hybrid composite structures [18], there is no systematic study to either consider the effect of all of the above mentioned contributing parameters on the behaviour of composite laminates or directly compare the behaviour of aerospace grade GFRP and CFRP with the same epoxy matrix under quasi-static indentation tests. Such a study would also contribute to understanding the effects of hybridization.

Therefore, this paper aims to address such a gap in the literature by carrying out a comprehensive experimental study on the effects of fibre properties in impact behaviour of laminated composites. For this purpose, a series of scaled tests were performed on QI S-glass/8552 epoxy covering scaling of in-plane dimensions and full three-dimensional scaled cases. The effect of fibre properties was studied by comparing experimental data obtained from the S-glass/8552 epoxy laminates with the results reported for IM7-carbon/8552 epoxy laminates for the same scaled quasi-static indentation tests [14]. The load–displacement behaviour and damage mechanisms of the IM7-carbon/epoxy laminates and S-glass/epoxy laminates were compared with each other. In addition, non-destructive techniques including ultrasonic scans (C-scan) and X-ray computed tomography (CT-scan) were employed to provide a detailed assessment of the damage evolution.

Table 1
Material properties of IM7-carbon/8552 epoxy and S-glass/8552 epoxy prepregs.

Material	IM7-carbon/8552 epoxy [21,22]	S-glass/8552 epoxy [19,23]
E_{11}(GPa)	161	47.7
E_{22}(GPa)	11.4	12.3
G_{12}(GPa)	5.17	4.83
G_{IIC}(N/mm)	0.8	1
Poisson's ratio (υ_{12})	0.3	0.28
Cured ply thickness (mm)	0.125	0.155
Areal weight (g/m^2)	134	190
Strain to failure (%)	1.62	3.87
Resin type	8552	8552
Manufacturer	Hexcel	Hexcel

2. Experimental method

2.1. Material and stacking sequence

Laminates were made from Hexcel S-glass/8552 epoxy prepreg and were compared with IM7-carbon/8552 epoxy laminates reported in [14]. Properties of these unidirectional glass and carbon prepregs are included in Table 1. The laminates have a quasi-isotropic (QI) stacking sequence, $[45_m/0_m/90_m/-45_m]_{ns}$ with varying values of m and n depending on the type of scaling as shown in Fig. 1. Three different types of scaling were used in this study; in-plane scaling (IS), ply scaling (PS), and sub-laminate scaling (SS). IS, PS and SS laminates had the recommended ASTM [20] sample dimensions of 150 × 100 mm (length × width). The reference (R) laminates were based on dimensions scaled down by a factor of two from the standard dimensions to 75 × 50 mm. For R laminates, the sequence was set to $m = 1$ and $n = 2$, i.e. $[45/0/90/-45]_{2s}$. For PS laminates, the thickness of each ply was doubled ($m = 2$, $n = 2$), i.e. $[45_2/0_2/90_2/-45_2]_{2s}$. For SS laminates, the overall thickness of the laminate was doubled ($m = 1$, $n = 4$), i.e. $[45/0/90/-45]_{4s}$. The indenter diameter was scaled with the in-plane dimensions. A summary of the types of laminates tested and their respective dimensions is shown in Fig. 1.

2.2. Manufacturing process

Different manufacturing stages of the laminates are shown in Fig. 2. The plies were laid-up manually to fabricate the laminates. The laminates where then put on Aluminium tool plates and were vacuum bagged under a constant 0.1 MPa pressure. The tool plates were placed in the autoclave and the laminates cured at the recommended curing cycle of 8552 epoxy resin at 110 °C for 60 min followed by 180 °C for 120 min under a constant 0.69 MPa pressure [20]. The laminates were cut to the specified dimensions using a tile cutter. Finally, each laminate was sprayed with a speckle pattern, see Fig. 2f, on its back face in order to measure the displacement and strain values using a Digital Image Correlation (DIC) system.

2.3. Test setup

Rectangular fixtures were utilised for the indentation testing. For the SS, PS and IS samples the fixture had a 125 mm × 75 mm window while for the R samples a 62.5 mm × 32.5 mm window size was used. This setup closely followed the ASTM D7136/D7136M recommended method of testing [20]. Quasi-static indentation tests were carried out on an Instron 8872 servo-hydraulic testing machine with a displacement rate of 1 mm/min, and a 16 mm diameter hardened steel indenter (8 mm for the R case) attached to a 25 kN load cell.

2.3.1. Data collection devices

Throughout the indentation tests, various data were recorded to

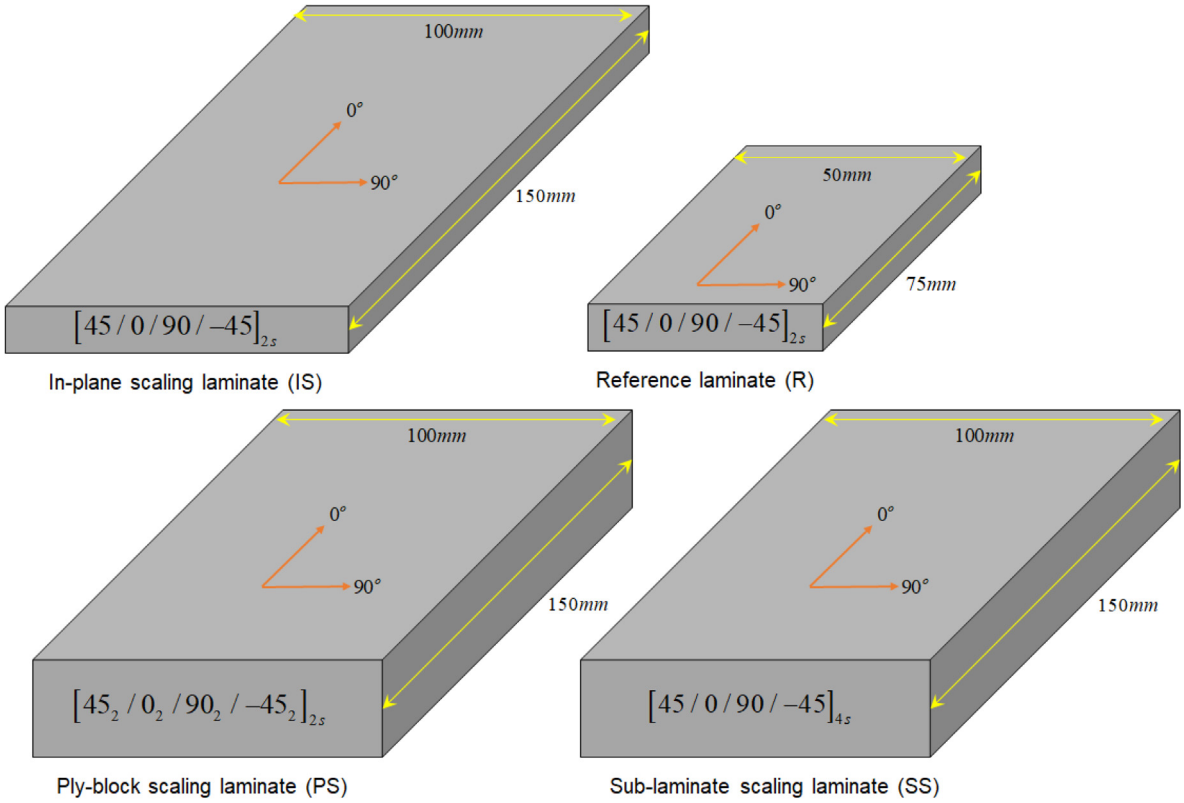

Fig. 1. The geometry and angle of each ply in the layup is shown for R, IS, PS and SS laminates.

facilitate characterization of the damage evolution of the laminates. Load and displacement data were recorded using a 25 kN load cell at a rate of 20 Hz using the Instron Wave Matrix Software.

Strain fields on the back surface of each sample were measured using an Imetrum digital image correlation system by correlating speckle pattern images. These images were taken by a pair of 5-mega-pixel cameras at 1 Hz. A mirror placed at 45° below the windowed fixture as shown in Fig. 3, provided a reflection of the back surface of the sample. Pointing the cameras at 45° to the mirror allowed images of the back surface to be taken during the test.

2.3.2. Non-destructive tests

2.3.2.1. Ultrasonic scans. The indented specimens were scanned using the ultrasonic immersion system provided by USL Ultrasonic Sciences with a 10 MHz transducer. Software provided by USL enabled gates to be set accurately, separating the front and back wall echoes of each specimen. Depth sandwiching brass blocks were used to lift the specimens off the bottom of the tank as shown in Fig. 4a. This helped to reduce echo from the bottom of the tank, preventing false signal acquisition. These scans were aimed at detecting the presence of delamination and providing details on the size of each delamination.

2.3.2.2. X-ray scans. The samples interrupted immediately after the first load drop and before the final failure were sent for X-ray Computed Tomography (CT) scanning. Through CT scans, a 3D view of the damage occurring within each ply was obtained. This was not possible through ultrasonic scans, which only showed delamination area.

In advance of carrying out the CT-scans, the following procedure was followed:

- A hole of size 0.5 mm was drilled at the centre of each specimen as shown in Fig. 4b. A small drill bit was used to reduce the possibility of any drill induced damage to the samples.
- The samples were then soaked in zinc iodide solution for at least 7 h as shown in Fig. 4c.

Small voids resulting from transverse cracks, matrix cracks and delamination were filled with zinc iodide through the soaking process. Exposure to X-rays illuminated this solution which helped to improve clarity of the scans within these damaged regions.

3. Results and discussion

3.1. Overall behaviour

The quasi-static indentation test allows investigation to be done at different load levels by interrupting the tests at different stages as the material is indented until it fails. Fig. 5a shows the overall behaviour of the S-glass/epoxy samples that were loaded until fibre failure at their back face due to tension. These indentation tests provide important information on the propagation and evolution of damage and the degradation mechanisms through analysis at different plies and different depths of the material. Therefore, all the samples were interrupted at 4 different load levels along the loading curve to characterize their damage evolution. A typical representative load–displacement graph for the SS S-glass/epoxy sample with four different test scenarios, interrupted at 4 different stages, is illustrated in Fig. 5b and described as follows:

- Stage 1 is associated with linear behaviour in the early stage of the loading process with an elastic response, and no underlying delamination damage in the laminate. One specimen was interrupted at the end of the linear part (Interrupted displacement 1), to see if there was any damage at this stage. For IS laminates, there is a nonlinear behaviour from the early stage of the loading, which can be attributed to the membrane stiffening effect as discussed in [14].
- Stage 2 is related to the initiation and propagation of delamination,

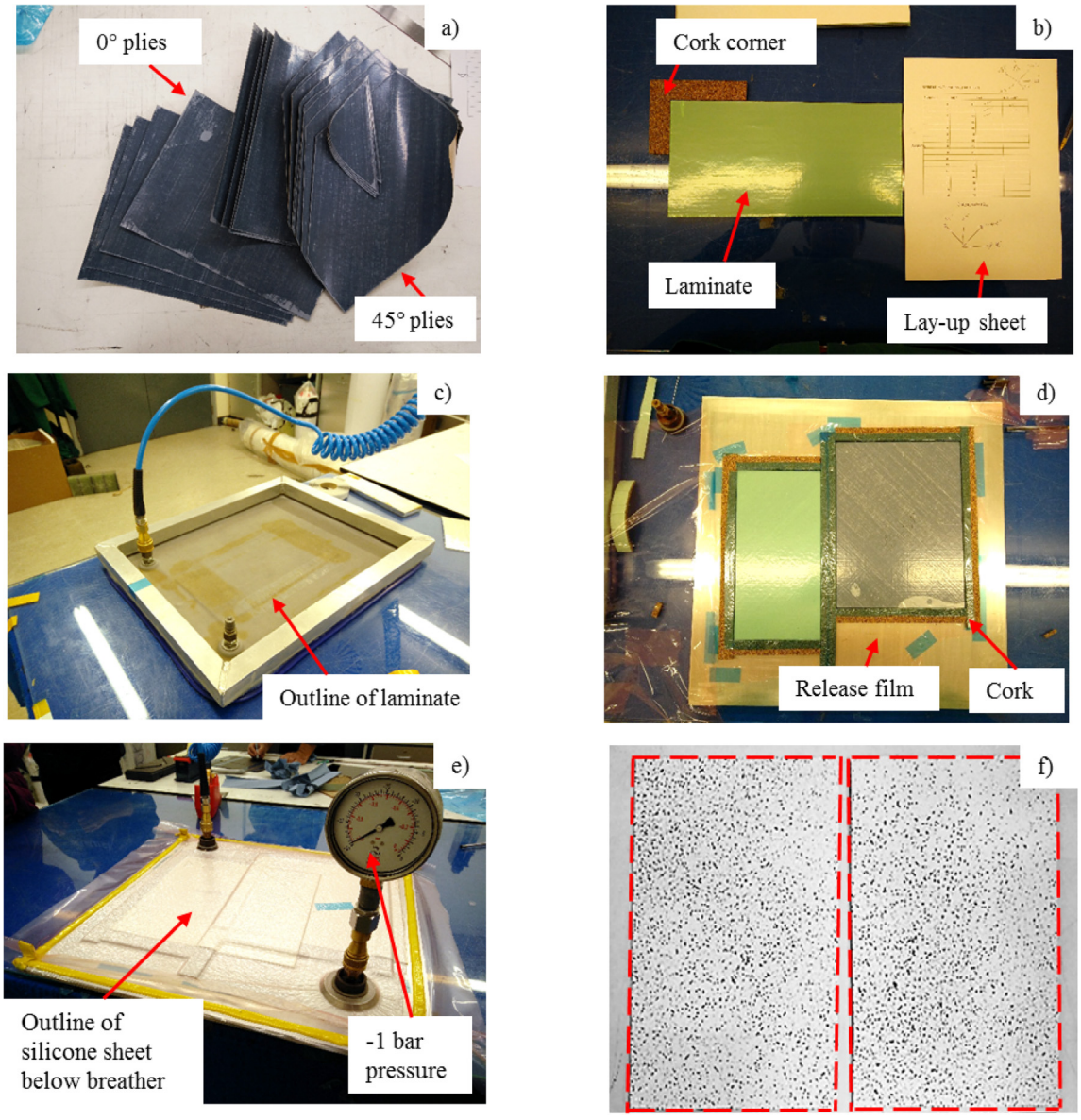

Fig. 2. Summary of the main steps involved in the fabrication of test specimens.

resulting in a loss in local rigidity. This is signalled by an evident change in rigidity (i.e. the slope of the load/displacement curve), whichever the laminate thickness. With increasing load in Stage 2, the number and size of delaminations increases. One specimen was interrupted immediately after the first load drop or evident change in slope (Interrupted displacement 2) and the other one was interrupted just before the maximum load (Interrupted displacement 3) to see the damage evolution.

- In stage 3 there are load-drops due to fibre failure at the back face of the specimen that is under tension. One specimen was loaded until this stage (Interrupted displacement 4).

The investigated S-glass/epoxy laminates in this paper have identical in-plane dimensions as the corresponding configurations that were studied before by Abisset et al. [14] for the IM7-carbon/epoxy laminates, but the thickness of the glass laminates in this study is 24% higher than that of the carbon laminates in Abisset's work owing to the higher ply thickness (see Table 2). Due to the higher thickness, the responses cannot be directly compared, and the maximum load level experienced by the S-glass/epoxy laminates is higher than the IM7-carbon/epoxy, see Fig. 5. Hence, in order to have a fair comparison between the mechanical behaviour of the glass and carbon laminates, the results were normalized by a thickness scaling rule extracted from previously published works. For thickness scaled plates (with the same in-plane dimensions), studying the contact between a rigid sphere and a laminate, some researchers [24,25] demonstrated that the elastic Hertzian contact law could be successfully applied. As stated by this law, the diameter D of the contact zone is given by

$$D \propto \sqrt[3]{F} \tag{1}$$

where F is the applied indentation force. From equilibrium considerations, it follows that the average punch shear stress along the specimen thickness at the boundary of the contact zone is

$$\tau = \frac{F}{\pi D h} \tag{2}$$

where h is the laminate thickness. Assuming that the shear stress is responsible for delamination initiation, from Eqs. (2) and (3) F_i is stated as

$$F_i \propto (\overline{\tau} \times h)^{1.5} \tag{3}$$

where $\overline{\tau}$ is the inter-laminar shear strength of the material. Based on

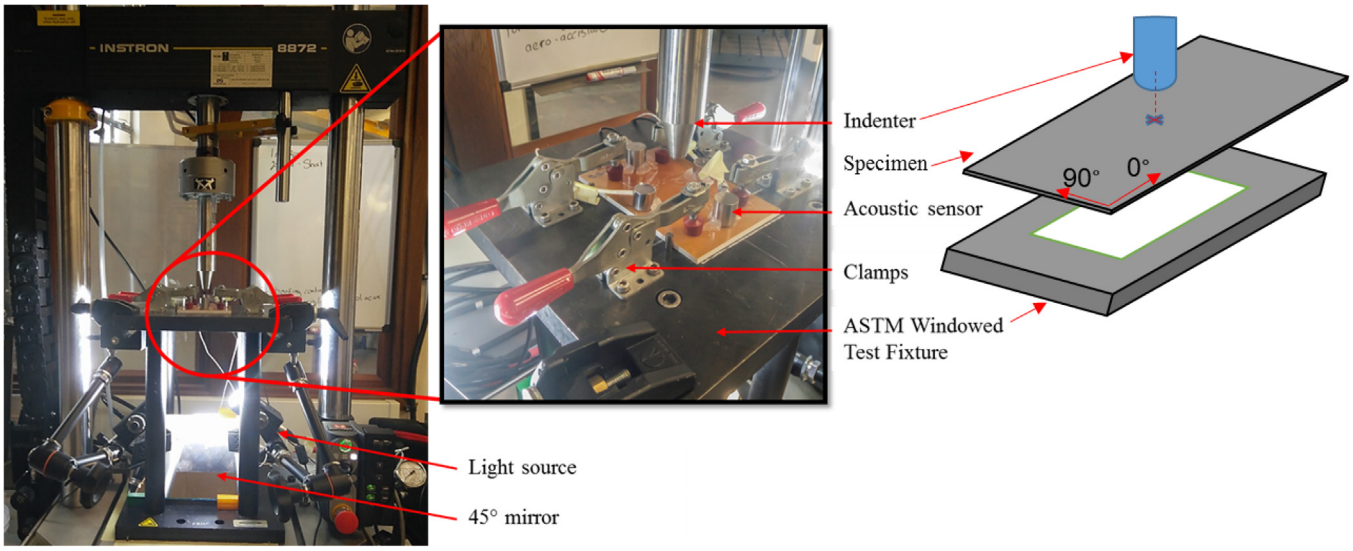

Fig. 3. Test setup for 150 × 100 mm samples with 16 mm indenter.

Eq. (3), it can be concluded that the load/displacement curves recorded for the different thicknesses should sensibly superpose with each other when the forces are scaled to the power 1.5, i.e. $R^{1.5}$, where R is the thickness ratio, and the displacements are held unchanged [15].

As reported by Davies et al. [2], the first load drop (or the evident change in the slope of the load/displacement curve) is mainly due to delamination initiation and can be evaluated by Eq. (4).

$$F_i = \frac{2\pi}{3}\sqrt{\frac{2E_{eff}h^3G_{IIC}}{1-\upsilon^2}} \tag{4}$$

where F_i is the critical threshold load for delamination initiation, E_{eff} is the effective homogenized Young's modulus of the laminate in bending, G_{IIC} is the mode II critical energy release rate, h is the laminate thickness, and υ is the laminate Poisson's ratio. Therefore, the load associated with delamination initiation depends not only on the thickness ratio $R^{1.5}$, but also on the critical energy release rate G_{IIC} and the Young's modulus of the laminate as indicated by Eq. (5).

$$F_i \propto E_{eff}^{0.5}G_{IIC}^{0.5}h^{1.5} \tag{5}$$

Therefore, the applied scaling approach is only valid for delamination initiation when the product of G_{IIC} and the Young's modulus of the laminates is the same. Consequently, there are limitations in the scaling approach using equation (3) in this paper to compare dissimilar materials, and it is applied here just to match the thicknesses of the S-glass/epoxy with the IM7/epoxy laminates for a fair comparison taking account of the most important mechanisms.

In order to validate this scaling rule, the experimental load–displacement results obtained for the investigated S-glass/epoxy laminates and IM7-carbon/epoxy laminates [14], with identical in-plane dimensions, are scaled using this scaling rule and the results are illustrated in Fig. 6. In addition, to check efficiency of this scaling rule for the laminates with less thickness differences, a 3 mm thick IM7-carbon/8552 epoxy laminate with stacking sequence of $[45/0/90/-45]_{3s}$, indicated as legend "A" in Fig. 6., was also manufactured and tested with identical procedures as the IM7/8552 epoxy laminates. As can be seen from Fig. 6, the scaling rule gives more realistic results for the IM7-carbon/epoxy laminate with 3 mm thickness that is scaled to 4 mm thickness, compared with the scaled 2 mm IM7-carbon/epoxy laminate. The scaling factors ($R^{1.5}$) are 1.54 and 2.82 for the former and the latter, respectively. This shows that the larger the thickness difference, the higher becomes the effect of uncertainties and nonlinearities in the adopted scaling approach. Hence, it can be concluded that when the thicknesses of the laminates are close to each other, this scaling rule is reasonable to use for comparisons. This is the case in this paper, where, as listed in Table 3, the investigated S-glass/epoxy laminates are only 24% thicker than the carbon laminates, so the load values for the S-glass/epoxy will be multiplied by the scaling factor of 0.72 (=(2/2.48)$^{1.5}$) to make a fair comparison between the glass/epoxy and carbon/epoxy laminates. It should be noted that the thickness scaling approach is just a simplified method to make the results comparable

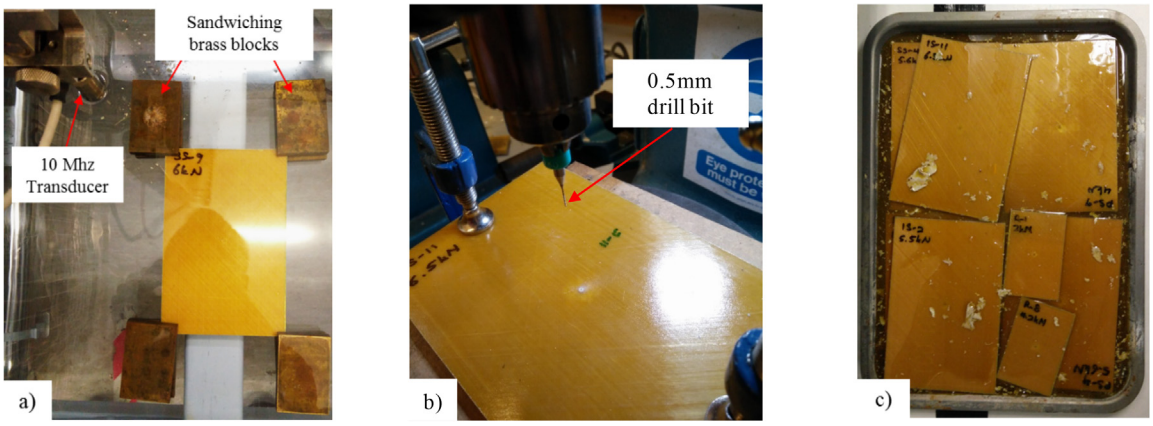

Fig. 4. a) Top view of the C-scan tank; b) Drilling the centre of a tested sample using a 0.5 mm drill bit; c) Dye penetrant bath of drilled samples.

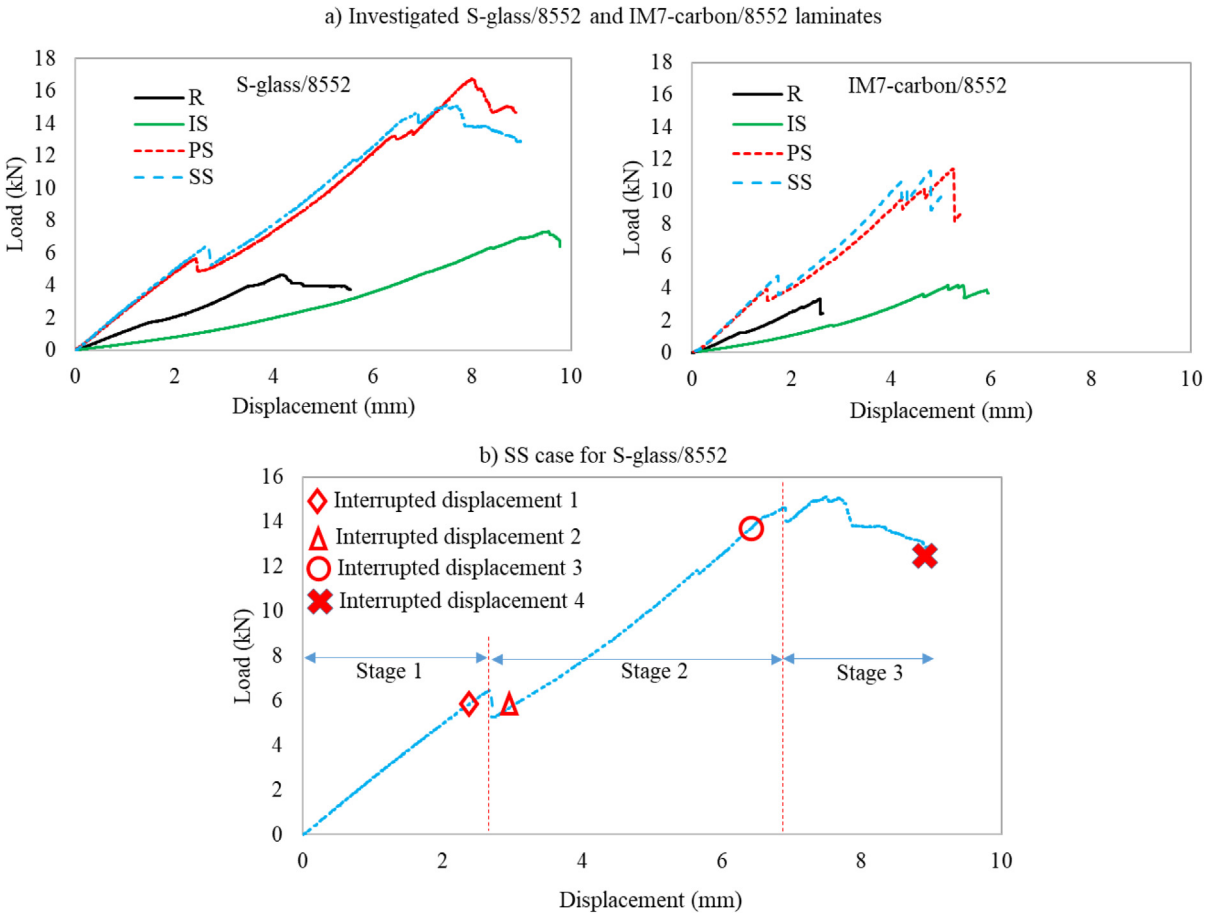

Fig. 5. Typical load–displacement responses for the samples under quasi-static indentation. a) all the tested cases until fibre failure on the back face, b) SS case, and highlighted points illustrate the displacement levels where the tests were interrupted.

and the scaled method is not completely valid for scaling the nonlinear response of the laminate and the various damage mechanisms, etc., across all the different laminate configurations.

As discussed above, the 2.48 mm IS and R cases of the glass laminates are scaled to match the 2 mm thickness of the carbon laminates whereas the 4.96 mm SS and PS cases of the glass laminates are scaled to match the 4 mm thickness of the carbon laminates. For the scaling, the load is multiplied by the ratio of the thickness to the power of 1.5 ($F \times R^{1.5}$) and the displacement remains the same. The scaled results of S-glass/epoxy and the experimental results of the IM7-carbon/epoxy laminates [14] are illustrated in Fig. 7. As shown in Fig. 7, a similar qualitative response can be observed for the stages 1–3 (introduced in Fig. 5) for both carbon and glass laminates. In the first stage, for most cases, except for Fig. 7b, load increases linearly until a critical load (F_i) followed by a first load drop. After the load drop, in the second stage, load goes up to more than twice the magnitude at the load drop. Once a second threshold is reached, a series of damage events generate a number of subsequent load drops. The tests were stopped when significant fibre failure in the lower ply was observed. It is worth noting that both carbon and glass laminates demonstrate a distinguishable load drop or change in the slope of the load/displacement curve, for stage 1 in R, PS and SS test cases. However, unlike the carbon laminates, there is no evident change in the slope of the load/displacement curve for IS test case in the glass laminates.

Some main characteristics of the raw experimental results for the IM7 [14] and the scaled results for the S-glass/epoxy, are summarized in Table 4. The initial slope and maximum displacement are mainly dependent on the fibre direction properties and are different for the S-glass/epoxy and IM7-carbon/epoxy laminates. Due to higher stiffness of the carbon fibres compared to the glass fibres (see Table 1), the initial stiffness of the carbon laminates is 1.66, 1.65, 1.24 and 1.71 times higher than that of the SS, PS, IS and R glass laminates, respectively.

As evidenced by many researchers [7,14,24,26] the first load drop depends on the critical energy release rate G_{IIC} and the effective Young's modulus of the laminate, and can be calculated by Eq. (4). Using the values listed in Table 2, the effective homogenized Young's modulus of the laminate which is used to evaluate the critical threshold load for delamination initiation is listed in Table 6. The effective homogenized modulus is derived from a simplified linear shell FE model, where the laminate is idealised as an elastic orthotropic plate

Table 2
A summary of the specimens used for quasi-static indentation tests.

Lay-up	m	n	Plate thickness Glass/epoxy (mm)	Plate thickness Carbon/epoxy (mm)	In-plane dimensions (a × b) (mm)	Indenter diameter (mm)
Reference (R)	1	2	2.48	2	75 × 50	8
In-plane scaling (IS)	1	2	2.48	2	150 × 100	16
Ply-block scaling (PS)	2	2	4.96	4	150 × 100	16
Sub-laminate scaling (SS)	1	4	4.96	4	150 × 100	16

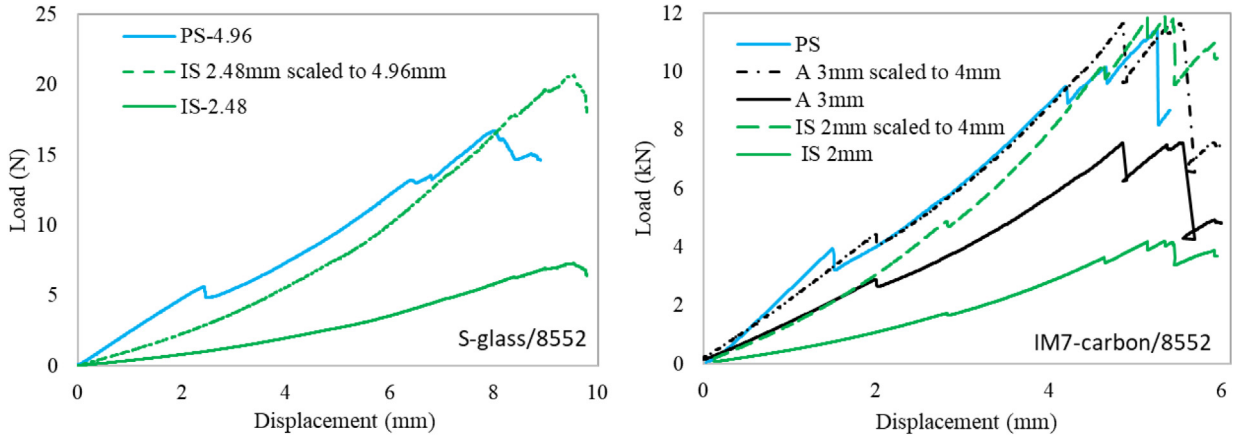

Fig. 6. The scaled experimental results obtained, using the introduced scaling rule as [15], for the S-glass/epoxy laminates with IS of thickness 2.48 mm scaled to SS and PS (4.96 mm thickness); and the IM7-carbon/epoxy laminates with IS 2 mm and A 3 mm thicknesses that are scaled to PS and SS (4 mm thickness). The layup sequence for the 3 mm carbon (A) is $[45/0/90/-45]_{3s}$.

under indentation, the Young's modulus value was varied until the FE model gave a similar stiffness as that in the experiment. As can be seen from Table 6, due to the lower values of the effective Young's modulus for the glass laminates, the analytically calculated critical load values are slightly lower for these laminates, compared with the carbon laminates. However, the experimental critical load values are very similar for the glass and carbon laminates. Furthermore, the experimental maximum load levels experienced by the carbon and glass samples (after scaling) are close to each other, except for the IS test case, see Fig. 7. The first drop is caused by initiation and immediate propagation of delamination at a number of different interfaces that resulted in the stiffness change. The load drops after the first load drop are mainly associated with delamination propagation. Later there was also some fibre breakage on the tension and compression sides of the composite laminates, as evidenced by front and back surface images and C-scan images taken from different stages of loading (presented later in section 3.3.). A similar damage scenario was reported in another study on quasi-static indentation of IM7/8552 epoxy laminates with a quasi-isotropic layup [27], where both fibre failure and delamination were reported during propagation of delamination. The maximum load is controlled by fibre failure, and it appears at a larger displacement for the glass samples than the carbon samples, due to the lower stiffness and higher strain to failure of the S-glass fibres. Considering the scaled results, the percentage of the reduction in load at the first load drop for the glass laminates is slightly less than that of the carbon laminates. As detailed in section 3.3, the variation in the induced damage is the reason for this slight difference. The area under the load–displacement curve up to the maximum load, was used to compare the energy absorption capacity of the glass and carbon laminates (see Table 5). This was done for comparison purposes as it was not easy to stop the tests at the same level of damage. It is evident that the scaled S-glass/epoxy laminates demonstrate considerably higher energy absorption, with values of 1.59, 1.57, 2.20, 1.45 times more for the SS, PS, IS and R test cases, respectively. This is due to the lower stiffness and higher strain to failure of the S-glass fibres compared to the carbon fibres. In stages 1 and 2, the S-glass/epoxy laminates undergo more displacement at the same load level as the carbon. Moreover, the final failure of the carbon laminates at stage 3 is quite abrupt and brittle whereas S-glass/epoxy laminates demonstrate a more gradual failure. This is due to the difference in the size and type of the induced damage by changing the fibre type, as discussed in section 3.3. The SS and PS specimens have the maximum absorbed energy for the carbon and glass laminates, respectively. These laminates have the highest level of induced damage, as detailed in section 3.3.

3.2. Strain field

Utilizing the software provided by LabVision, digital image correlation was performed on the images taken by the cameras. This allowed to plot the displacement and strain fields near the failure of the specimens as shown in Fig. 8. The region of highest strain was a semi-circular area under the indenter showing the localized nature of damage in indentation. Analyzing the changes in surface strain values against 'time in Fig. 9, it is shown that changes in gradient or discontinuities in strain values occurred at a certain point during the loading of every configuration. By overlaying these plots with load-time graphs, it is found that these changes correspond to the point of the first load drop in most cases, corresponding with evident changes in rigidity, where delamination initiated. The maximum strains measured from the DIC slightly exceed the quoted strain to failure of the S-glass fibres (3.87%) from Table 1. The DIC measurement was interrupted earlier than the maximum load due to the appearance of damage on the back face of the samples, such as fibre failure and splitting due to delamination and matrix cracking.

3.3. Ultrasonic scan (C-scan)

Due to the semi-transparent property of the glass/epoxy, indentation induced delaminations near the top and bottom surfaces are visible as they change the appearance of the specimens. This observable damage is highlighted with a dashed box in each visual image shown in Fig. 10. The damage on the front face (compression side) of the glass

Table 3
Thickness scaling of S-glass/8552 epoxy laminates to match the thickness of IM7-carbon/8552 epoxy laminates studied in [11].

Scaling type	Glass laminates test thickness (mm)	Carbon laminates test thickness (mm)	Thickness ratio (R)	Scaling factor for displacements	Scaling factor for forces
R	2.48	2	0.806	1	$0.806^{1.5} = 0.72$
IS	2.48	2	0.806	1	0.72
PS	4.96	4	0.806	1	0.72
SS	4.96	4	0.806	1	0.72

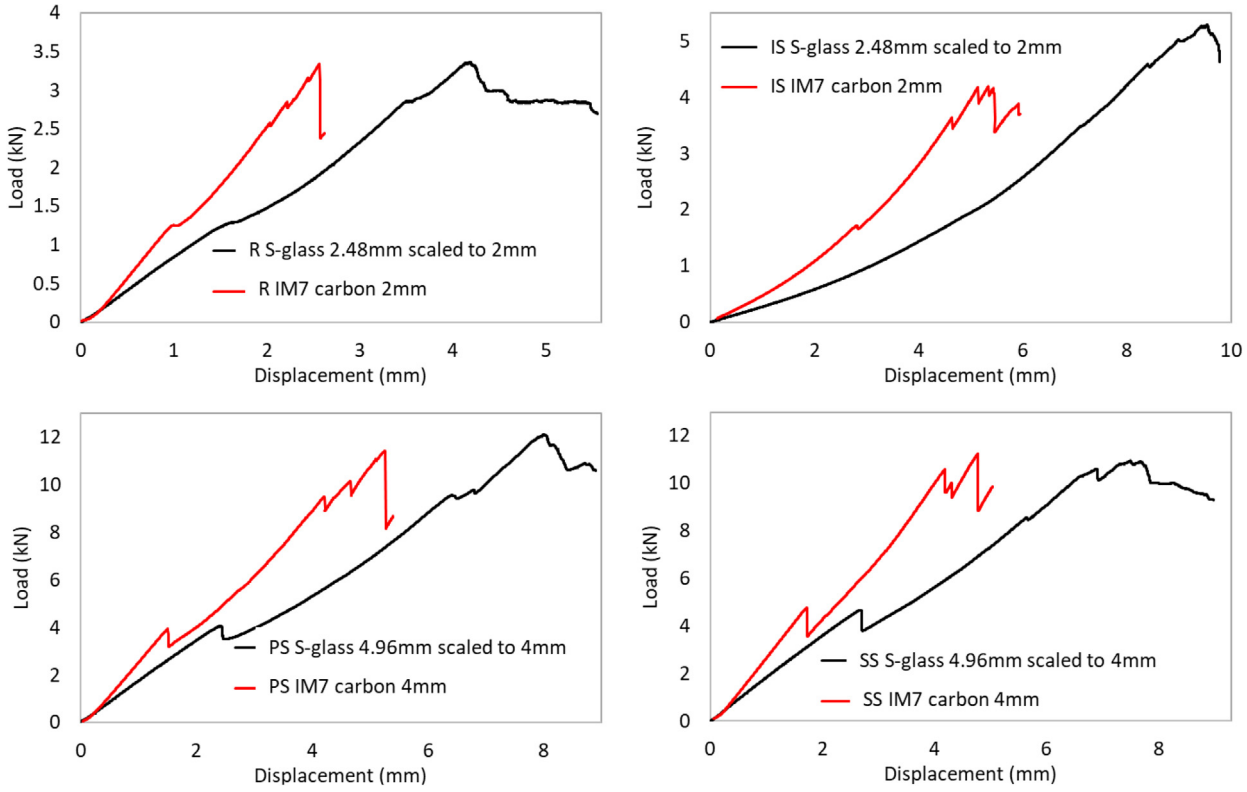

Fig. 7. Comparison of load–displacement traces between S-glass/8552 epoxy and IM7-carbon/8552 epoxy samples for R, IS, PS and SS test cases.

samples is a local dent with no fibre failure, whereas some fibre failure and splitting on the back face (tensile side) appears at a later stage when the load is close to the maximum load. The surface images of the IM7-carbon laminates are not reported in [14]. However in another study [27] on quasi-static indentation of IM7/8552 epoxy laminates with quasi-isotropic layup of $[60/0/\text{-}60]_{4S,}$ and the same dimensions as SS samples in [14], the samples indicated compression side failure from the early stage of the loading just after the first load drop, whereas the tensile side fibre failure appeared at a later stage when the load was close to the maximum load. It reflects a higher resistance to compression failure resistance of the S-glass compared with the IM7-carbon fibre composites.

Despite the translucence of the glass/epoxy samples, it remains difficult to visually determine the exact size of delamination. Hence, ultrasonic C-scan was applied for better assessment of the damage evolution in the composite laminates. C-scan images of the specimens are illustrated in Fig. 10 for various stages of the load–displacement curves. It should be noted that the un-scaled loads are reported in the discussion of damage mechanisms from the C-scan and the CT-scan results.

As shown in Fig. 10 for the S-glass/epoxy, no delamination is observed before the first load drop. Hence, no images are displayed. This is similar to the IM7-carbon/epoxy samples, see Fig. 11, where no damage was observed before the load drop [14]. Immediately after the first load drop, the size of delamination was measured and is compared with those of carbon as tabulated in Table 7. The size of delamination in the glass laminates is marginally larger compared to the carbon laminates for all cases except for the IS samples.

3.4. Analytical analysis for damage size prediction

The simplified analytical model proposed in [26] can be used to estimate the size of the delaminated area immediately after the load drop. The mid-plane displacement of the plate centre (ω_0) under the indentation force (F), given as Eq. (9) [26].

$$\omega_0 = \frac{FR_{eq}^2}{16\pi D*}(1 + (N^2 - 1)\beta^2) \tag{6}$$

where F is the applied load at the first load drop, $D* = E_{eff}h^3/12(1-\upsilon^2)$ is the equivalent bending stiffness of the laminate as reported in Table 6, N is the number of sub-laminates created by delaminations which are assumed circular, R_{eq} is the radius of the equivalent circular plate having clamped boundary conditions, and $\beta = r/R_{eq}$ is the non-dimensional delamination radius (r). Eq. (6) can be

Table 4
Some main characteristics of the investigated carbon and scaled glass laminates.

Laminate configuration	Carbon/epoxy				Scaled glass/epoxy			Carbon/Glass Stiffness ratio
	Thickness (mm)	Initial stiffness (kN/mm)	Displacement at the max load (mm)	Maximum load (kN)	Initial stiffness (kN/mm)	Displacement at the max load (mm)	Max load (kN)	
SS	4	2.98	4.78	11.19	1.79	7.73	10.94	1.66
PS	4	2.87	5.25	11.41	1.74	8.02	12.09	1.65
IS	2	0.47	5.43	4.18	0.38	9.55	4.96	1.24
R	2	1.47	2.56	3.31	0.86	4.19	3.36	1.71

*Glass loads are scaled by Eq. (3).

Table 5
Comparison between first load drop and energy absorption of the carbon and scaled glass laminates.

Laminate configuration	Thickness (mm)	First load drop								Max load	
		load level (kN)		Displacement (mm)		Load drop (%)		Energy absorbed kN.mm)		Energy absorbed (kN.mm)	
		Glass*	Carbon	Glass	Carbon	Glass*	Carbon	Glass*	Carbon	Glass*	Carbon
SS	4	4.66	4.73	2.68	1.7	18.6	24.6	6.24	4.02	42.18	26.48
PS	4	4.06	3.96	2.42	1.5	13.24	21.0	4.91	2.97	47.46	30.19
IS	2	N/A	1.7	N/A	2.8	N/A	3.74	3.57	2.38	22.23	10.12
R	2	1.29	1.28	1.61	1.0	0.0	3.54	1.04	0.64	5.98	4.13

*Glass loads and energy values are reported from Fig. 7, where the loads are scaled by Eq. (3).

Table 6
Comparison of critical load for delamination obtained from experiment and analytical solution for the carbon and scaled glass laminates.

Test case	υ	h (mm)	E_{eff} (GPa)	G_{IIC} (N/mm)	Theoretical F_C (kN)	Experimental F_C (kN)*	*% difference*
R-glass	0.28	2	26.8	1	1.43	1.29	−10.8
R-carbon	0.3	2	42.0	0.8	1.61	1.28	−25.8
IS-glass	0.28	2	26.8	1	1.43	N/A	N/A
IS-carbon	0.3	2	42.0	0.8	1.61	1.70	5.3
PS-glass	0.28	4	26.8	1	4.04	4.06	0.2
PS-carbon	0.3	4	42.0	0.8	4.55	3.96	−14.9
SS-glass	0.28	4	28.4	1	4.65	4.66	0.2
SS-carbon	0.3	4	51.6	0.8	5.05	4.73	−6.8

*Glass loads are scaled by Eq. (3).

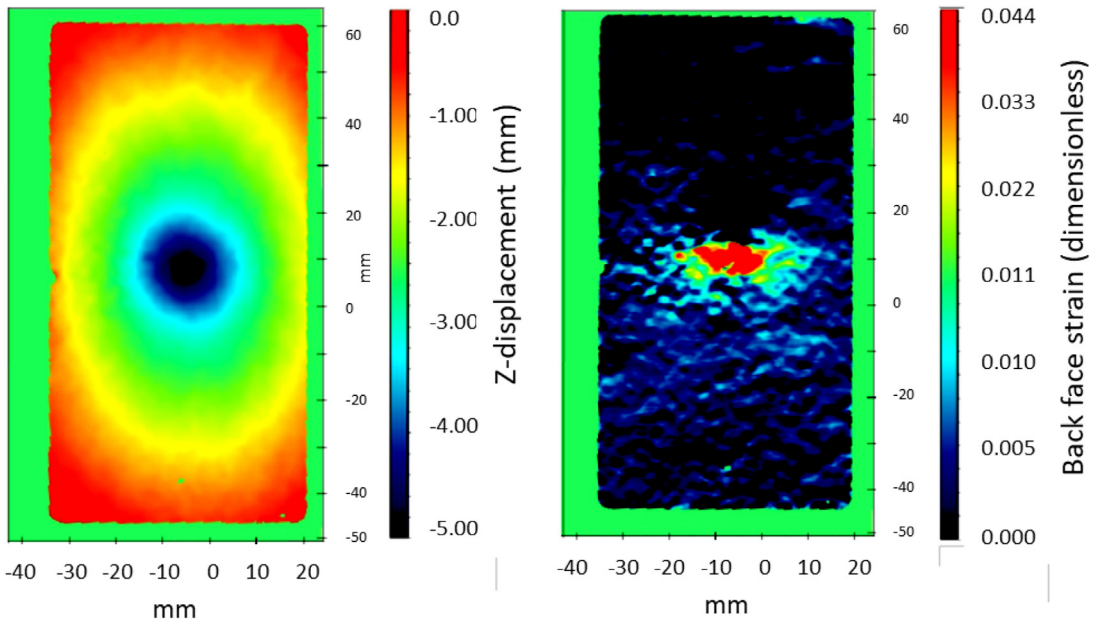

Fig. 8. A typical displacement in the loading direction, *Z*-displacement (left) and back surface strain, plotted for the SS S-glass/epoxy laminates at the point of failure.

re-written for the delamination radius as:

$$r = \sqrt{\frac{16\omega_0\,\pi D * - FR_{eq}^2}{(N^2-1)F}} \tag{7}$$

The ratios of glass delamination radius (r_G) to carbon delamination radius (r_C) at the first load drop can therefore be obtained using Eq. (8).

$$\frac{r_G}{r_C} = \sqrt{\frac{\frac{16\omega_{0iG}\pi D_G^* - F_{iG}R_{eq}^2}{F_{iG}}}{\frac{16\omega_{0iC}\pi D_C^* - F_{iC}R_{eq}^2}{F_{iC}}}} \tag{8}$$

To be consistent with the carbon laminates [14], R_{eq} for the large (the Is, Ps and Ss cases) and the R glass laminates was corrected to 70 mm and 35 mm, respectively. These values of R_{eq} for the rectangular shaped plates were calculated by modifying the size of a circular plate in order to fit the deflection field of the simply supported rectangular plate by comparing two analytical solutions as detailed in [28]. Using Eq. (8), the calculated (r_G/r_C) values are tabulated in Table 8 and are compared with the measured delamination radius in Table 7. In general, there is a reasonably good correlation between the analytical and experimental delamination ratios for SS and PS laminates, however the analytical value for R laminates overestimates that of experiment by 46%.

The linear model predicts that the propagation of delamination takes place at a constant load F which depends on the plate's material and geometrical parameters as well as on the number of circular delaminations [26]. The general expression for N-1 delaminations as given in Eq. (9) is:

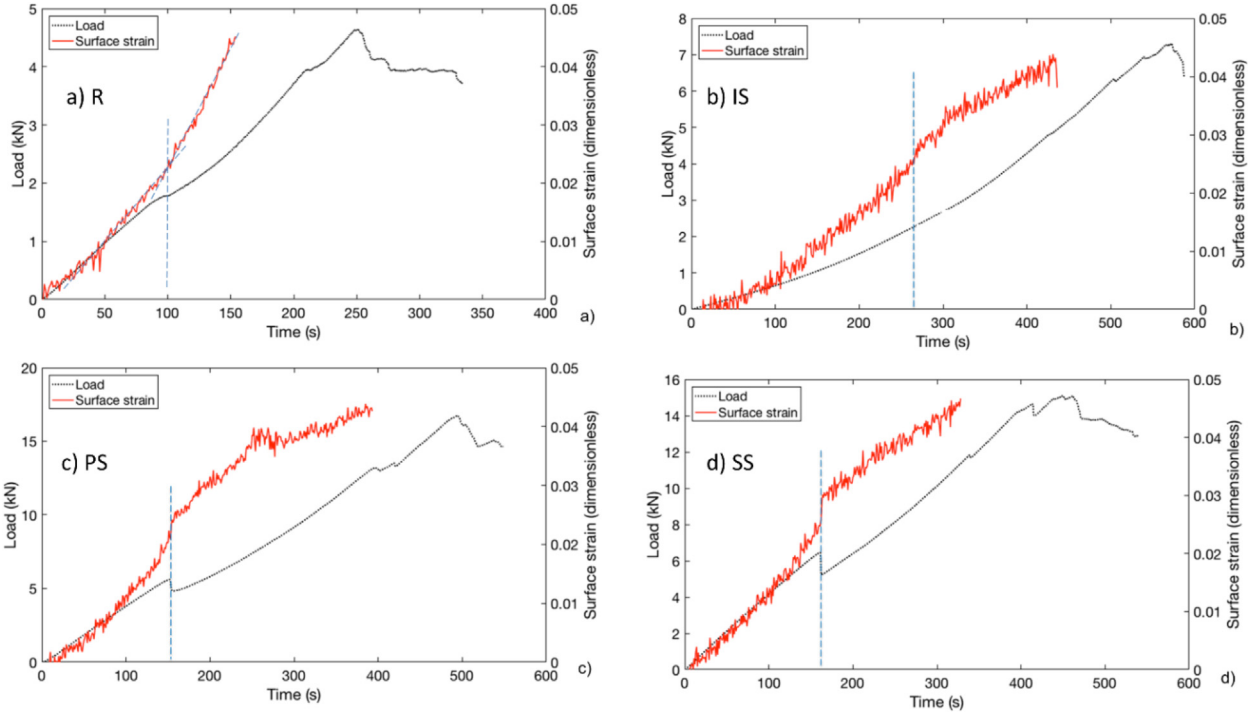

Fig. 9. The applied load and surface strain at the center of the specimen was plotted against time for the S-glass/epoxy laminates.

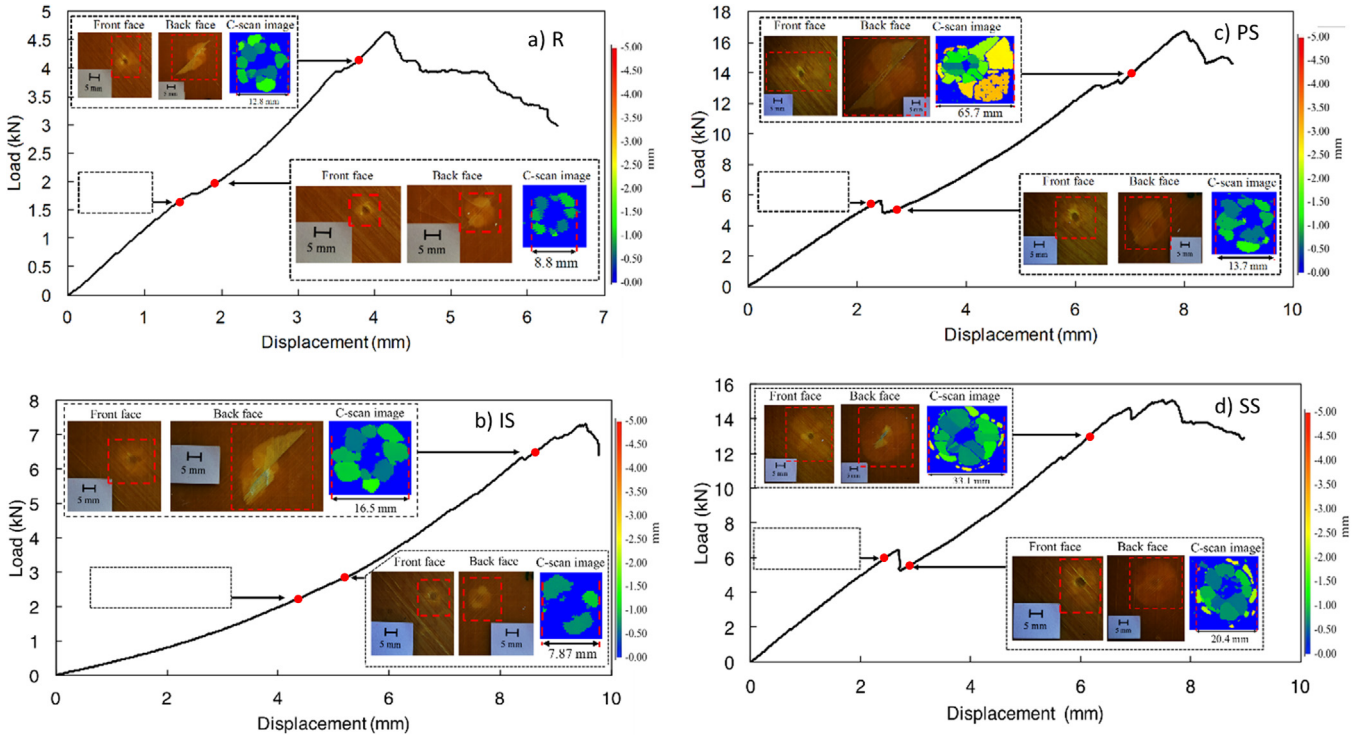

Fig. 10. Front and back surface images and C-scan images at each interruption was shown for the S-glass/epoxy; a) R, b) IS, c) PS, d) SS samples.

$$F = \sqrt{\frac{32\pi^2 D^* G_{IIC}}{N+1}} \tag{9}$$

An estimate of the load drop value for the investigated samples can be obtained by considering N = 2 for the critical load (F_i), at which the first load drop occurs, and N = 5 for the force at the end of the unstable load drop (F_2). $N = 2$ was selected at the first load drop, as a single central delamination is expected to firstly initiate at the mid-plane of the plate with the maximum shear stress, creating two sublaminates. N = 5 was selected according to the laminate configurations (considering 4 central delaminations creating five sublaminates) and in consistency with the analytical calculations for the carbon laminates [14]. This yields

$$\Delta F = F_i - F_2 = \sqrt{\frac{32\pi^2 D^* G_{IIC}}{3}} - \sqrt{\frac{32\pi^2 D^* G_{IIC}}{6}} = 0.29\sqrt{\frac{32\pi^2 D^* G_{IIC}}{3}} = 0.29F_i \tag{10}$$

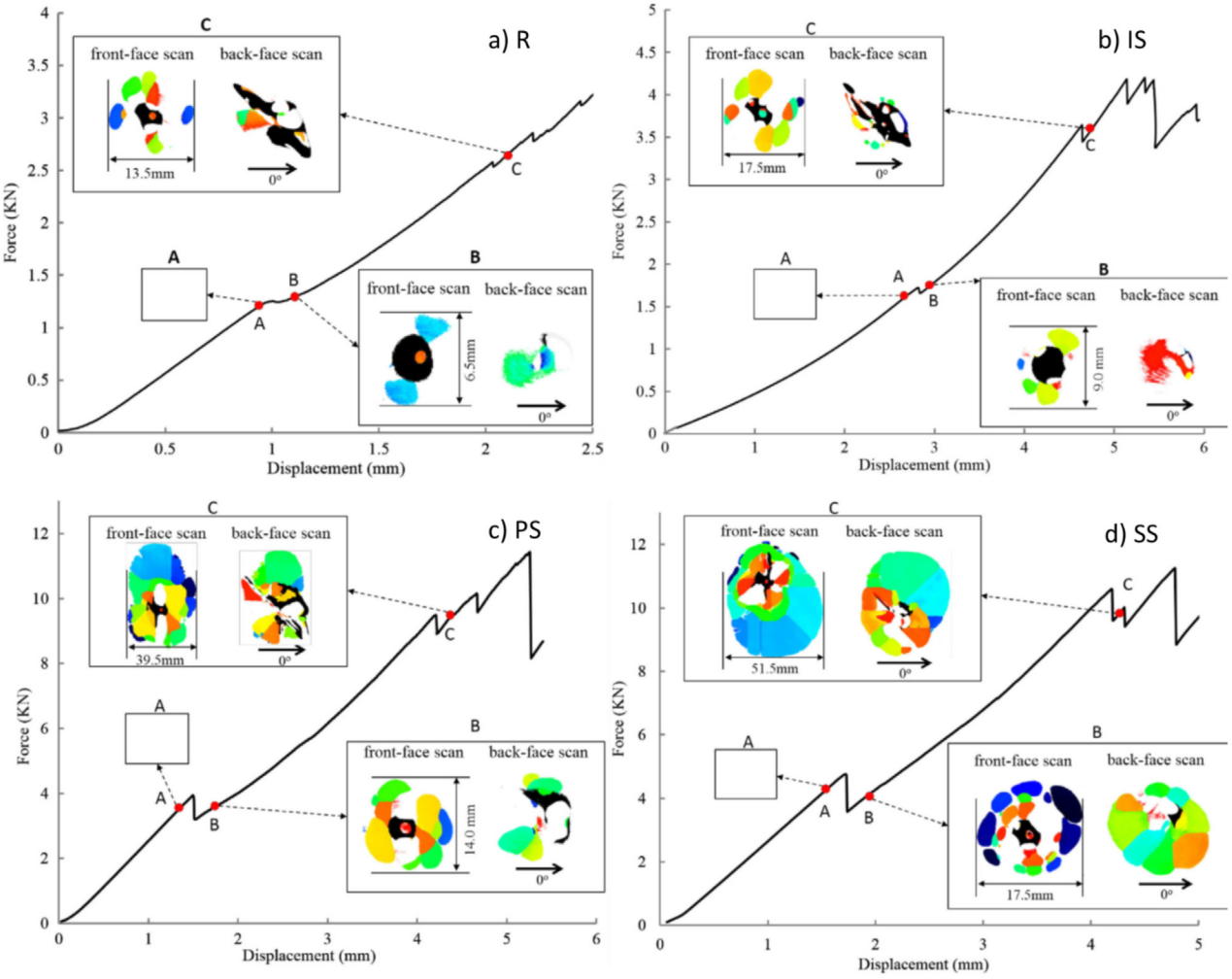

Fig. 11. Representative global load–displacement curve and C-scans depicting the overall delamination width for the IM7-carbon/epoxy [14].

Table 7
Comparison between glass and carbon laminates on delamination initiation and propagation. The values are taken from the indicated points in Figs. 10 and 11. The delamination diameters are calculated from projected areas, assuming circular delaminations, rather than direct measurements.

Laminate configuration	First delamination, first load drop				Delamination propagation, second load drop			
	Delamination diameter (mm)		Delamination area (mm^2)		Delamination diameter (mm)		Delamination area (mm^2)	
	Glass	Carbon	Glass	Carbon	Glass	Carbon	Glass	Carbon
SS	20.4	19.5	326.8	300.0	33.1	51.5	860.5	2083.1
PS	13.7	13.5	147.4	142.5	65.7	39.5	3390.1	1225.4
IS	7.87	8.5	48.6	57.1	16.5	17.5	213.8	240.5
R	8.8	6.6	60.8	34.2	12.8	13.5	128.7	143.1

Table 8
Comparison of analytical and experimental delamination size ratios after the first load drop for the glass and carbon laminates. C and G stand for the carbon and glass laminates. R_{eq} and r are the equivalent circular plate and delamination radius of the laminate, respectively.

Test case	R_{eq} (mm)	D^*_G/D^*_C	Theoretical r_G/r_C	Experimental r_G/r_C
SS	70	1.04	1.09	1.04
PS	70	1.21	1.08	1.01
IS	70	1.21	0.74	0.92
R	35	1.21	1.98	1.33

Table 9
Comparison of analytical and experimental delamination size ratios for the PS and R samples, after the first load drop for the glass and carbon laminates.

Delamination diameter ratio	Experimental Glass	Theoretical Glass	Experimental *Carbon*	Theoretical Carbon
PS/R	1.56	2	2.05	2

$$F_2 = \sqrt{\frac{1}{2}} F_i = 0.71\, F_i \tag{11}$$

In the displacement driven test, the value of ω_0 before and after the load drop is the same, one can write Eq. (6) as.

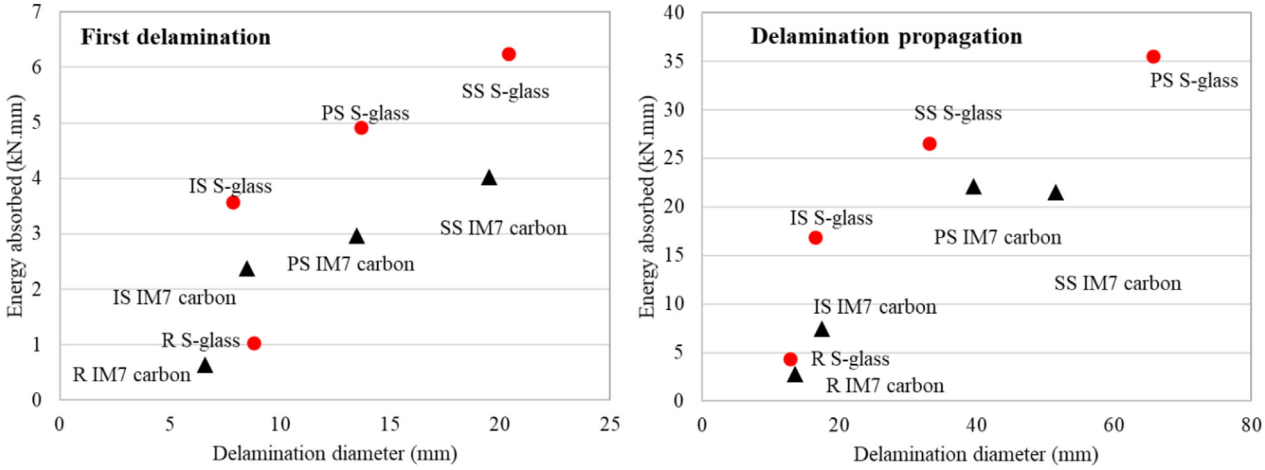

Fig. 12. Delamination diameter versus the absorbed energy for the investigated laminates for the first load drop (first delamination) and after the second load drop (delamination propagation). The presented energy values are calculated at the indicated points in Figs. 10 and 11, by measuring the area under the load–displacement curves in Fig. 7. The damage size are the un-scaled results from Table 7.

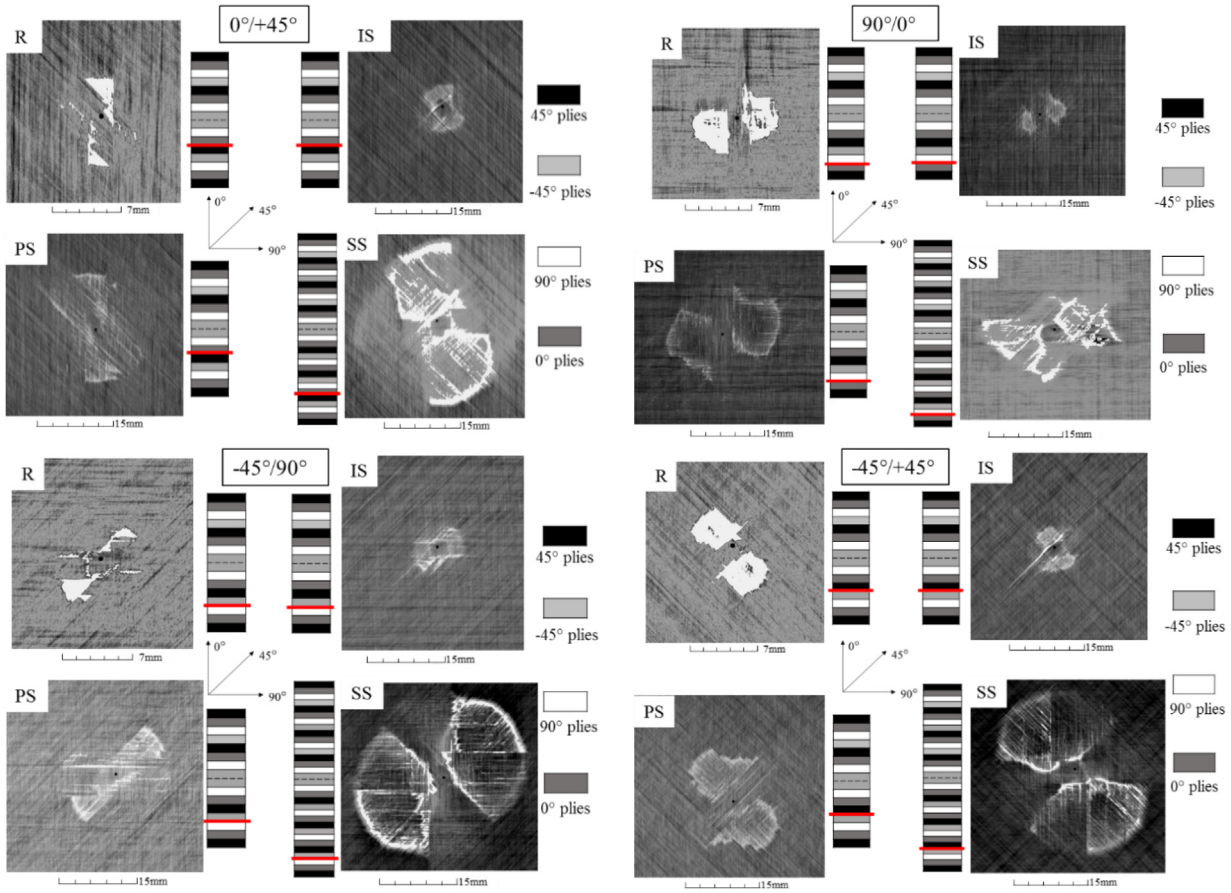

Fig. 13. Delamination at the four respective interfaces 0°/45°, 90°/0°, −45°/90° and 45°/−45° for each S-glass/8552 epoxy configuration. The specific interface where the image was taken is highlighted in red.

$$\frac{F_i R_{eq}^2}{16\pi D*}(1 + (N^2 - 1)\beta^2) = \frac{F_2 R_{eq}^2}{16\pi D^*}(1 + (N^2 - 1)\beta^2) \tag{11}$$

Using Eq. (11), and assuming the initial delamination behaviour and N = 2 on the left hand side and N = 5 on the right hand side of Eq. (10), it gives:

$$\frac{F_i R_{eq}^2}{16\pi D^*}(1 + 3\beta^2) = \frac{0.7 F_i R_{eq}^2}{16\pi D^*}(1 + 24\beta^2) \tag{12}$$

Eq. (12) can be solved for the delamination size;

$$\beta = \frac{r}{R_{eq}} = 0.14 \tag{13}$$

According to Eq. (13), the delamination size should scale with the in-plane plate dimensions. Table 9 compares the analytical and experimental delamination size ratios (using Eq. (13) and Table 7) for the true scaled pair, that is the R and the PS plates. For the first delamination, Eq. (13) appears to give a reasonable value for the carbon

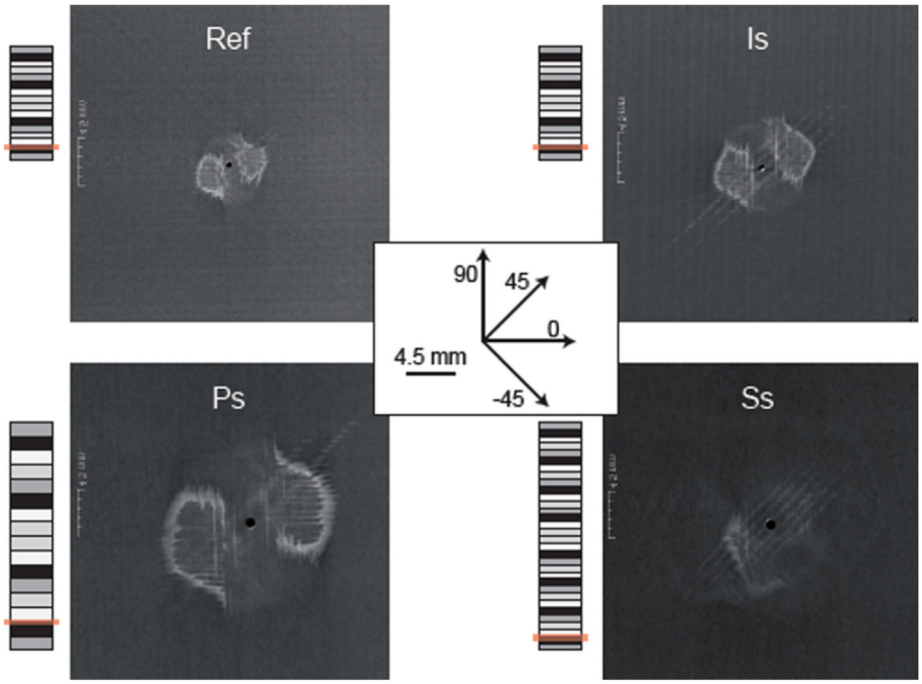

Fig. 14. Delamination after the first load drop on the bottom 90/0 interface for the four test cases of the IM7-carbon/epoxy [14]. The specific interface where the image was taken is highlighted in red.

samples, however it overpredicts it by about 28% for the glass samples. This reflects the dependency of the delamination size scaling on the laminates' constituents, indicating the limitation of the applied scaling approach.

Fig. 12 illustrates the size of delamination for the carbon and glass laminates at the first load drop and after the second load drop. For all the cases, the glass samples absorb more energy than the carbon samples, despite having a similar delamination size. IS and R have similar values of delamination size for the carbon and glass laminates whereas there is a discrepancy for the SS and PS laminates. For the first delamination, SS sample has the highest delaminated area and absorbed energy for both glass and carbon samples. However, for the propagation stage, for the carbon laminates, the SS sample has the highest delaminated area and absorbed energy, whereas, for the glass laminates, the PS sample has the highest delamination area and absorbed energy. The displacement and load levels for the PS glass are much higher compared with the SS glass sample at the second load drop, making it difficult to make direct comparisons for the damage size.

3.5. X-ray computed tomography scans (CT-Scans)

CT-scans on each configuration after the first load drop showed similar transverse crack patterns and shape of delamination for the glass/epoxy and carbon/epoxy laminates. Two delaminations, symmetrically positioned with respect to the indenter, develop at each interface, their shape and orientation determined by the fibre directions in the adjacent plies. As examples, Fig. 13 shows the delamination pattern at four different interfaces (0°/45°, 90°/0°, −45°/90°, 45°/−45°) in each configuration through the thickness of the laminates. It was deduced that for interfaces where the difference in adjacent ply angle was 45°, a triangular shaped delamination was formed. Similarly, with a difference in ply angle of 90°, a peanut shaped delamination was formed, elongated in the direction of the fibres in the lower ply. These observations match with the findings reported for the IM7-carbon/epoxy laminates [14], see for example the bottom 90/0 interfaces in Fig. 14, whereas delaminations shaped as a peanut develop at 90° interface where fibre directions are different by 90°.

Key observations found from the CT-scans indicated that the damage mechanism in the S-glass/epoxy and IM7-carbon/epoxy laminates have a similar pattern, but a different size. The key observations from the CT-scans are summarised in the following:

- Delamination at each interface was controlled by the direction of transverse cracks.
- Delamination propagation occurred parallel to the fibre direction of the bottom ply and normal to the fibre direction of the top ply.
- Delamination was symmetrical about the fibre direction of the bottom ply.
- The combined delamination at each interface forms the shape of a circle.
- No delamination occurred on the first interface.
- Presence of transverse cracks between two adjacent interfaces allowed delamination to step through the thickness.
- Lengths of matrix cracks and delamination area were larger on the bottom half of the samples.

4. Conclusions

The aim of this study was to investigate the effect of fibre properties in indentation behaviour of laminated composites. A comprehensive series of scaled tests were compared on QI S-glass/8552 epoxy and QI IM7/8552 epoxy laminates covering scaling of in-plane dimensions and full three-dimensional scaled cases. The following items are concluded:

- The mechanical results were normalized by a thickness scaling rule to have a fair comparison between the S-glass laminates that were thicker than the IM7-carbon laminates. It was found that when the thickness of the laminates is close to each other, this scaling rule is reasonable to use for comparisons. This is the case in this paper, where, the investigated glass laminates are only 24% thicker than the carbon laminates.
- Due to the ability of S-glass/8552 epoxy laminates to sustain higher deflections prior to failure compared to the IM7-carbon/epoxy laminates, and the similar load levels experienced by the laminates, the energy absorption of the glass laminates was almost 2 times higher than that of the carbon, showing a better potential of the

glass laminates for energy absorption purposes, compared to the carbon counterparts.

- The damage on the compression side of the glass laminates is a local dent with no fibre failure, and some fibre failure and splitting on the back face near the maximum load. The IM7-carbon laminates however indicated compression side failure from the early stage of the loading just after the first load drop, whereas the tensile side fibre failure appeared at a later stage when the load was close to the maximum load. The different damage evolution affected the load–displacement behaviour, where the percentage of the reduction in load at the first load drop for the scaled glass laminates is slightly less than that of the carbon laminates. Moreover, the final failure of the carbon laminates is quite abrupt and brittle whereas the S-glass/epoxy laminates demonstrate a more gradual failure.
- Analysing results from the C-scan and CT-scan images showed no difference in overall damage mechanisms between the glass and carbon samples. Both laminates showed the same shape of delaminations at respective interfaces with the presence of transverse cracks. The C-scanning showed a similar delamination size in the glass/epoxy and carbon/epoxy laminates immediately after the first load drop, however the delamination size for the propagation stage was dependent on the layup sequence and the fibre properties.
- The analytical damage size scaling model predicted that the delamination size should scale with the in-plane plate dimensions. This scaling approach appears to give a reasonable value for the carbon samples, however it overpredicts it by about 28% for the glass samples. This reflects the dependency of the delamination size scale on the laminates' constituents, indicating the limitation of the applied scaling approach. Further numerical investigation is required to explain the experimental results in more detail, beyond the simplified models used in this paper.

Declaration of Competing Interest

The authors declare that they have no known competing financial interests or personal relationships that could have appeared to influence the work reported in this paper.

Acknowledgements

This work was funded under the UK Engineering and Physical Sciences Research Council (EPSRC) Programme Grant EP/I02946X/1 on High Performance Ductile Composite Technology in collaboration with Imperial College, London. The authors acknowledge Hexcel Corporation for supplying materials for this research. The data necessary to support the conclusions are included in the paper.

References

[1] Cantwell WJ, Morton J. The impact resistance of composite materials – a review. Composites 1991.
[2] Davies GAOAO, Zhang X. Impact damage prediction in carbon composite structures. Int J Impact Eng 1995;16(1):149–70.
[3] Abrate S. Impact on laminated composites: recent advances. Appl Mech Rev 2009.
[4] Abrate S. Impact on composite structures. Cambridge University Press; 1998.
[5] Sun XC, Hallett SR. Barely visible impact damage in scaled composite laminates: experiments and numerical simulations. Int J Impact Eng 2017.
[6] Olsson R. Analytical model for delamination growth during small mass impact on plates. Int J Solids Struct 2010;47(21):2884–92.
[7] Sun XC, Wisnom MR, Hallett SR. Interaction of inter- and intralaminar damage in scaled quasi-static indentation tests: Part 2 - Numerical simulation. Compos Struct 2016;136:727–42.
[8] Richardson MOWOW, Wisheart MJJ. Review of low-velocity impact properties of composite materials. Compos Part A Appl Sci Manuf 1996;27(12):1123–31.
[9] Aoki Y, Suemasu H, Ishikawa T. Damage propagation in CFRP laminates subjected to low velocity impact and static indentation. Adv Compos Mater Off J Jpn Soc Compos Mater 2007.
[10] Kaczmarek H, Maison S. Comparative ultrasonic analysis of damage in CFRP under static indentation and low-velocity impact. Compos Sci Technol 1994.
[11] Cantwell WJ, Morton J. Geometrical effects in the low velocity impact response of CFRP. Compos Struct 1989;12:39–59.
[12] Yang FJ, Cantwell WJ. Impact damage initiation in composite materials. Compos Sci Technol 2010;70(2):336–42.
[13] Fuoss E, Straznicky PV, Poon C. Effects of stacking sequence on the impact resistance in composite laminates - Part 1: Parametric study. Compos Struct 1998;41(1):67–77.
[14] Abisset E, Daghia F, Sun XC, Wisnom MR, Hallett SR. Interaction of inter- and intralaminar damage in scaled quasi-static indentation tests: Part 1 – Experiments. Compos Struct Feb. 2016;136:712–26.
[15] Caprino G, Lopresto V, Scarponi C, Briotti G. Influence of material thickness on the response of carbon-fabric/epoxy panels to low velocity impact. Compos Sci Technol 1999;59(15):2279–86.
[16] Sutherland LS, Sá MF, Correia JR, Soares CG, Gomes A, Silvestre N. Quasi-static indentation response of pedestrian bridge multicellular pultruded GFRP deck panels. Constr Build Mater 2016;118:307–18.
[17] Yu B, Karthikeyan K, Deshpande VS, Fleck NA. Perforation resistance of CFRP beams to quasi-static and ballistic loading: The role of matrix strength. Int J Impact Eng 2017;108:389–401.
[18] Bulut M, Erkliğ A, Yeter E. Hybridization effects on quasi-static penetration resistance in fiber reinforced hybrid composite laminates. Compos. Part B Eng. 2016;98:9–22.
[19] Ratcliffe JG. Characterization of the Edge Crack Torsion (ECT) Test for Mode III Fracture Toughness Measurement of Laminated Composites," Nasa Tech. Memo., no. September; 2004.
[20] A. International, "ASTM D7136/D7136M-15 Standard test method for measuring the damage resistance of a fiber-reinforced polymer matrix composite to a drop-weight impact event; 2003.
[21] O'Brien TK, Johnston WM, Toland GJ. Mode II interlaminar fracture toughness and fatigue characterization of a graphite epoxy composite material, NASA Tech. Rep. NASA/TM-2010-216838; 2010.
[22] Hallett SR, Green BG, Jiang WG, Wisnom MR. An experimental and numerical investigation into the damage mechanisms in notched composites. Compos Part A Appl Sci Manuf 2009.
[23] de Cássia Mendonça R, Sales BL, Endo Rossi Dias, Donadon MV. Influence of temperature on interlaminar fracture toughness of a carbon fiber-epoxy composite material. Adv Mater Res 2016;1135:35–51.
[24] Yang S, Sun C. Indentation law for composite laminates. Composite Materials: Testing and Design (6th Conference). 2009.
[25] Tan TM, Sun CT. Use of statistical indentation laws in the impact analysis of laminated composite plates. J Appl Mech 2009.
[26] Suemasu H, Majima O. Multiple delaminations and their severity in circular axisymmetric plates subjected to transverse loading. J Compos Mater 1996;30(4):441–53.
[27] Saeedifar M, Najafabadi MA, Zarouchas D, Toudeshky HH, Jalalvand M. Clustering of interlaminar and intralaminar damages in laminated composites under indentation loading using Acoustic Emission. Compos. Part B Eng. 2018;144:206–19.
[28] Sun XC, Hallett SR, Suemasu H, Wisnom MR. Simplified analytical approximations for scaled composite laminates under transverse loading. Compos Struct 2020;236.